Experiments in Fluids 8, 59–71 (1989)

Experiments in Fluids

Experimental studies of model porous media fluid dynamics

A. P. Yarlagadda* and **A. P. Yoganathan**

Cardiovascular Fluid Mechanics Laboratory, School of Chemical Engineering, Georgia Institute of Technology, Atlanta, GA 30332, USA

Abstract. The three-dimensional, steady flow velocity components of a viscous, incompressible, Newtonian fluid in model porous media were measured. The model porous geometries were constructed from 3 mm glass rods. A laser Doppler anemometer was used to measure two of the velocity components and the third was calculated by integrating the continuity equation. The effects of viscous drag, inertial flow fields and eddy losses in the model were studied. The results showed that the measured flow was laminar and stable such that micromixing of the fluid was absent. Inertial flow effects were absent due to high viscous drag coefficients.

1 Introduction

Low Reynolds number fluid dynamics, in particular fluid dynamics in porous media, is a very fundamental topic for a wide variety of fields in applied science and engineering. Reviews by Greenkorn (1983), Scheidegger (1974), Happel and Brenner (1973), Bear (1972), Collins (1961), and Carmen (1956) present a clear picture of the research developments in these fields. Darcy's law (1856) is the first empirical equation to quantify the flow phenomena in porous media. Hudson and Roberts (1952) and Rose (1945) established the presence of two critical Reynolds numbers for flow in porous media. One, corresponding to Reynolds numbers above which the "linear law" is no longer valid, and the other for the onset of turbulent flow. Scheidegger (1974) showed how the first transition takes place due to inertial flow in curved tubes long before the onset of turbulence. Darcy's law is valid only before the first transition takes place. The flow phenomena become complex after the first transition. The empirical equation by Ergun (1952) relates the pressure drop and the flow rate in the absence of inertial effects and presence of eddies. Researchers, (e.g. Lin (1981) Keller (1976) and Coulaud et al. (1988), have been trying to model fluid flow through porous media. The success of these numerical models can be established only by comparing the model predictions with the experimental findings. But, experimental studies with porous media are very difficult for two major reasons. First, in such test materials, it is difficult to define the flow rates and flow geometry. Second, there is to date no experimental tool capable of making such quantitative measurements in such small scale flow fields. Hence, very few experimental data that quantify the flow velocity information in porous media are available in the literature. Rosenstein (1980) and Lin (1981) have made experimental studies in scaled-up models of few complex flow geometries. This paper is another such study aimed at generating 3-D flow velocity information in a model porous medium.

2 Experimental apparatus and methodology

2.1 The experimental apparatus

The model porous media used in this experimental study is shown in Fig. 1. The structure consists of three different types of 3 mm diameter glass rod arrangements; vertical glass rods and two different layers of horizontal glass rods arranged at a 60° angle to each other. The vertical glass rods were arranged in hexagonal layout, having a space of 3 mm between the rows of the vertical glass rods. The assembled model porous media has dimensions of $81 \times 57 \times 55.2$ mm^3, and it was enclosed in a 6.3 mm (1/4″) thick pyrex glass chamber having two opposite side surfaces open for through-flow of the test fluid. Two flow model geometries were constructed with this 3-D assembly of glass rods. In model 1 flow geometry the bulk flow was perpendicular to the rows of vertical glass rods. Therefore, the bulk flow direction of the fluid in model 1 studies was at an angle of 30° to the orientation of the glass rods present in the horizontal layers. In model 2, the other two side surfaces were left open. Therefore, the bulk flow direction of the fluid in model 2 was at an angle of 60° to the orientation of the glass rods present in the horizontal layers. Since the glass rod arrangement was systematic, it was clear that the test section was made of a representative cell geometry shown in Fig. 2a in model 1 porous medium and Fig. 2b in model 2 porous medium (both had average porosity of 0.438)

* Present address: Truman Medical Center, University of Missouri at Kansas City, Kansas City, MO 64108, USA

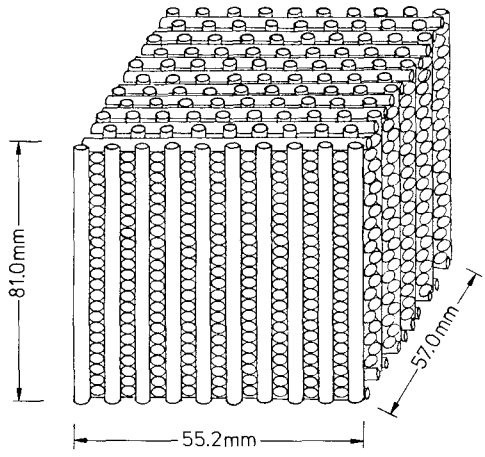

Fig. 1. Modular test cell made of glass rods

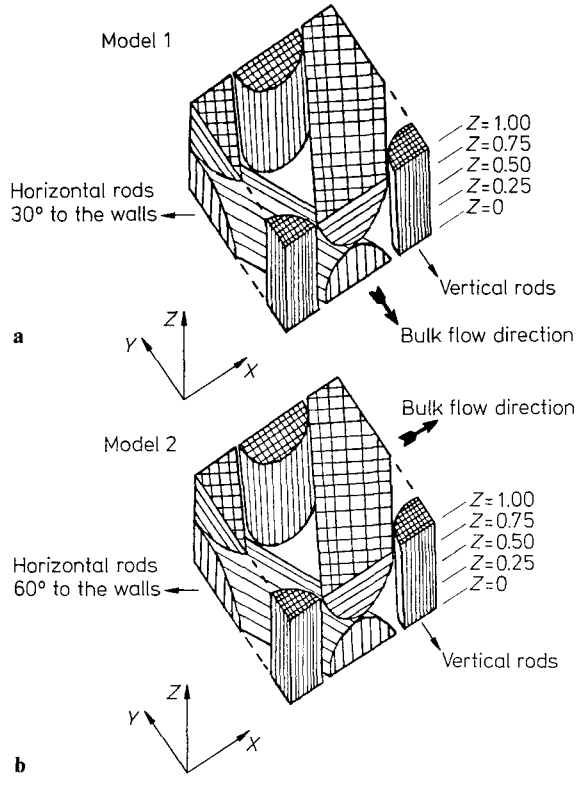

Fig. 2a and b. The structure of the representative cells

2.2 *Test fluids*

To avoid the wall effects and the entrance effects, velocity measurements must be made near the center of the model porous medium. Since a laser Doppler anemometer (LDA) system (which is an optical system) was used in these experiments, reflection and diffraction of the laser light had to be totally absent. To avoid such problems, a matched refractive index technique was used. In this technique, the test fluid was selected with a refractive index very close to that of the test

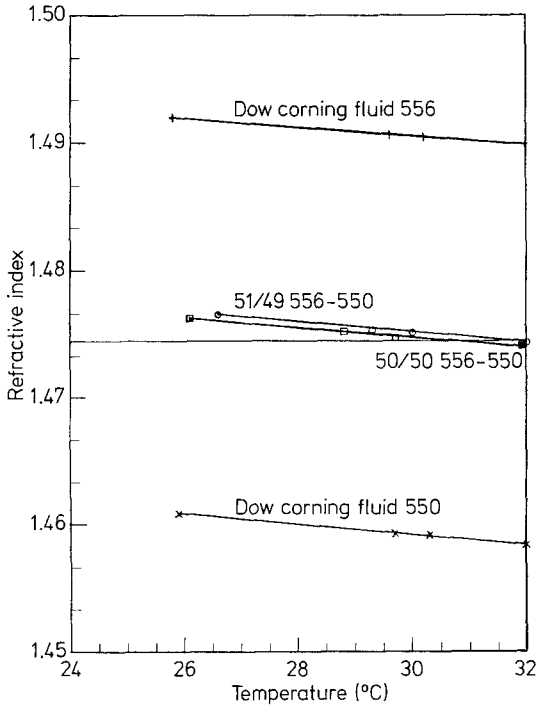

Fig. 3. Refractive index of the silicone fluids

section material (pyrex). Dow Corning 556 and 550, both being silicone fluids, have refractive indices above and below that of pyrex (1.474). These fluids mix well in all ratios, making it possible to prepare a blend with the required refractive index. Hand mixing of the fluids for a few minutes in a beaker was sufficient to make a homogeneous fluid blend. An Abbe refractometer (American Optical Company, Model No. 10450) was used to measure the refractive indices of the fluids at different temperatures. A synchro-electric viscometer (Brookfield, Model No. LVE) was used to measure the viscosities of the fluids at different temperatures. All the fluids showed Newtonian behavior (constant viscosity at different shear rates). Figures 3 and 4 depict the characteristic refractive index and the viscosity information of these fluids.

2.3 *Flow system*

Figure 5 is a schematic diagram of the flow system. It contains a nutating pump, (Gormann-Rupp Industries, Ohio, Model GRI/20810), a bypass loop, a rotameter, control valves, a surge tank, and the model porous media test section. The flow meter (Fisher and Porter, PA Model P5-1759) was first calibrated with the test fluid. To isolate the pump vibrations, the test section and the LDA were mounted on a vibration-free table (Ealing Vibration Isolation System Model No. 24-5316). The rest of the flow section was mounted separately on a heavy table. The test section was mounted on a traversing mechanism and was moved when-

ever it was necessary to relocate the LDA system probe volume inside the test section.

2.4 *Traversing mechanism*

The traversing mechanism was made of two sliding plates. These sliding plates had micrometer turn screw attachments, which advanced the sliding plate uniformly relative to the main frame. Two such frames were fixed together in such a way that the advancement of the sliding plates would be in orthogonal directions. The model porous medium test section was fixed to the sliding plate of the top frame and the sliding plate of the bottom frame was bolted to a laboratory jack. With this optical quality traversing mechanism the test section could be moved in horizontal plane with an accuracy of 10 microns. The test section was moved vertically by adjusting the level of the supporting jack. This third directional movement was measured by using a micrometer dial gauge (accuracy: 1 micron).

2.5 *Laser Doppler anemometer*

A three beam LDA (Disa Electronics, Franklin Lakes NJ) was used to measure the two components of the velocity fields in the model porous media. Since it was convenient to operate the LDA in the horizontal plane, the velocity components in the bulk flow direction and vertical direction were measured and the velocity component in the lateral direction was estimated. Figure 6 shows the schematic arrangement of the three beam LDA system used in this study. A 15 mW He-Ne laser having a wavelength of 632.8 nm was used. The laser beam first passed through two retarders (DISA X20) that were mounted on the optical system. The first retarder plate converted the linearly polarized laser light into circularly polaized laser light. The second retarder converted the circularly polarized light into linearly polarized light, with correct polarization direction relative to the optical axis. The beam then entered the beam splitter (DISA X25) where it was split into two beams of equal intensity. One of these two beams, the main laser beam passed through a glass rod to maintain the same optical path length as the other beam which passed through the Bragg cell. The Bragg cell, an acousto-optic modulator, introduces a fixed optical frequency shift $f_0 = \pm 40$ mHz to the laser beam that passed through it. This beam was then split into two beams which were polarized in planes perpendicular to each other, and at an angle of 45° to the plane of polarization of the main beam. The main beam combined with each of the component beams formed a separate set of fringe patterns. A particle crossed the fringes of the measuring volume caused separate Doppler frequencies in the two polarization planes, which were separately received by two photomultiplier tubes that were set to receive signals in the two different planes of polarization. The scattered light had a frequency of $f_{pm} = f_0 + f_d$, where f_d, was the Doppler frequency caused by the movement of particles. The signal was then sent to

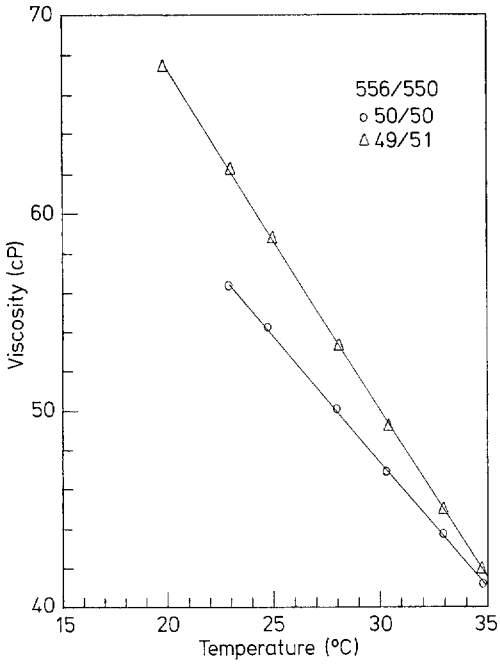

Fig. 4. Viscosity of the silicone fluid blends

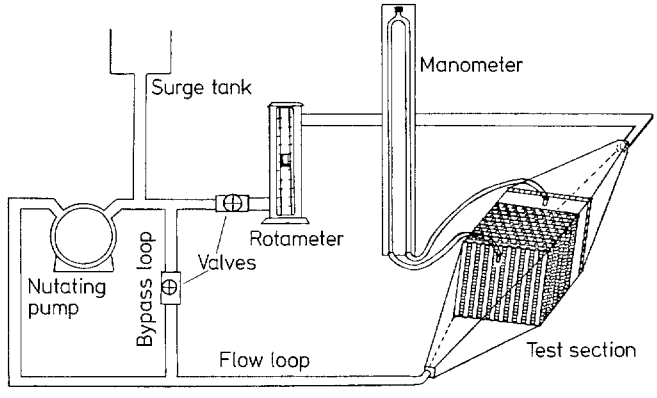

Fig. 5. Schematic diagram of the flow system

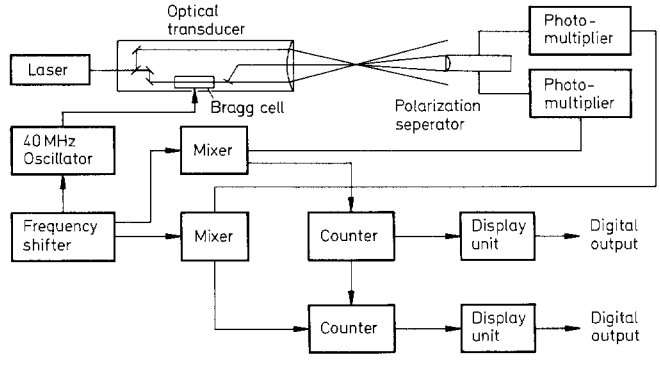

Fig. 6. Block diagram of the laser Doppler anemometer

two frequency shifters (DISA 55 N10 LDA frequency shifters) and mixed with a variable frequency shift signal. The output signal was then fed to the counters (DISA 55L90a LDA counter processor). The incoming signal was preamplified to 25 dB and then passed on to an attenuator which might be varied between 0 and − 31 dB by means of the amplifier gain selector buttons. The signal was amplified and passed through a variable band-pass filter. The filtered signal was applied to a Schmitt trigger, and then fed to a count sequencer which used 500 MHz clock pulses to get a digital representation of the frequency. The mean frequency was calculated by the DISA 55L94 Mean Velocity Computer. A DISA 55L91 Data Rate module indicated the rate, and the number validated on groups of 1,000 points. In addition, the instantaneous digital signal was available at two digital I/0 ports of the counter main frame. The digital output from the counter was interfaced with a PDP 11/03 mini-computer via a DISA 57G20 Buffer interface. The measured velocity information was transferred to floppy discs for storage and further data processing.

2.6 Experimental methodology

Experiments were conducted by creating a steady flow through the two open faces of the model. Due to the complex geometry of the model porous medium, a three dimensional flow field was created. Since the test section was made of representative cell geometry (Fig. 2 a and b), a representative cell located at the center of the model porous medium was selected for the experimental studies. Further, it was reasonable to assume that entrance effects and wall effects were absent in the flow fields of these representative cells. First the experiments were begun with 50–50 silicone fluid blend. The flow system was run sufficient time to ensure that it would reach a study fluid temperature. The pumping device and the frictional forces caused a rise in temperature of the test fluid which was compensated by thermal losses to the surroundings at the steady state conditions. At this working condition, a close matching of the refractive index of the fluid and the pyrex was achieved by adding Dow Corning 556 fluid in small quantities. The first approximation of the quality of the match was judged visually by the degree of invisibility of the glass rods in the fluid blend. The exact judgement was made by allowing the laser beams to pass through different sections of the test section without being disturbed. A good match of the refractive indices was verified by testing the coherence and the optical quality (such as intensity, plane of polarization, etc.) of the laser beams after they had been passed through the test section.

Velocity measurements were done at a number of grid locations of the representative cell. Experiments were carried out at 5 different Z levels as shown in Fig. 3 in a sequential fashion. Two of the velocity components (bulk flow directional and vertical directional) were simultaneously measured at each of the several nodes of a three dimensional grid volume. First, for fixed Y and Z coordinates, measurements were made at increments of 0.25 mm along the X-axis, then the probe volume was moved by 0.25 mm laterally, and experiments were repeated. Once the velocities at grid points in an X, Y-plane were measured, the probe volume was then moved to another vertical level and the procedure was repeated.

Approximately one thousand data samples were collected at each of the 1,600 mesh locations spread out over 5 different levels of the representative cell. The weighted average (based on the time each particle spent in the probe volume) of each component was considered. The data collection software of the LDA system was run by a PDP-11/03 minicomputer, and the data were stored on floppy disc. The velocity field information was processed after the conclusion of the experiment. The vibration-free table, the matched refraction or refractor index technique, and the forward scatter mode of LDA operation all improved the experimental conditions resulting in a high signal-to-noise ratio. The two measured vectors of the 3-D velocity field at each grid point were stored on a magnetic tape in a sequential fashion. Experiments were conducted at four different flow rates (all < 30 ml/s) in both model geometries (Fig. 2).

3 Data presentation and the third component estimation

The experimental data were analyzed and presented in 3-D graphical form. Each of the measured directional velocity fields were plotted at each level of the model geometry. Figure 7 is a sample 3-D graph of the bulk fkow directional velocity component plotted on an X-Y plane which corresponds to 0.25 level (Fig. 2) of the model 1 representative

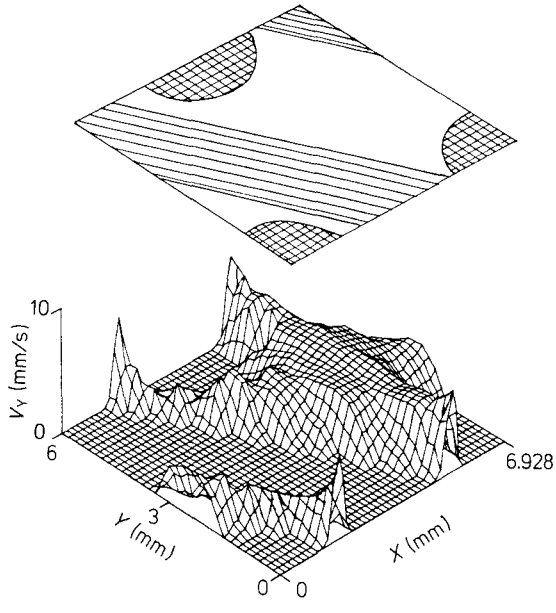

Fig. 7. Bulk directional velocity component at 0.25 level of model 1 ($Re = 0.327$)

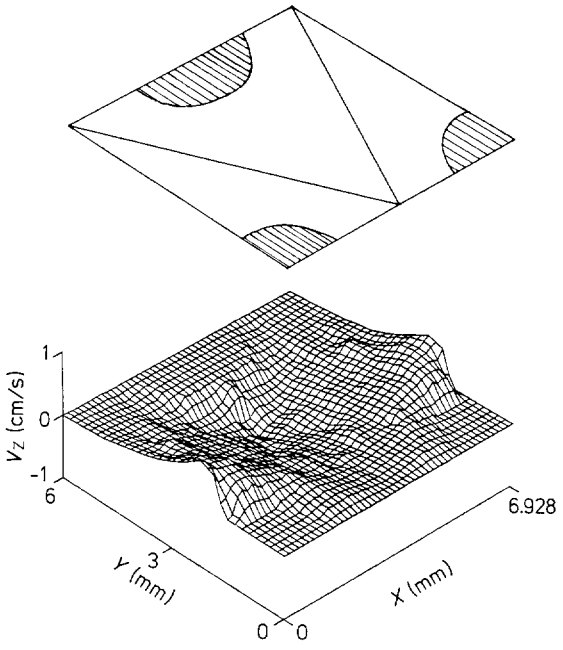

Fig. 8. Vertical directional velocity component at level 0.5 of model 2 ($Re = 1.914$)

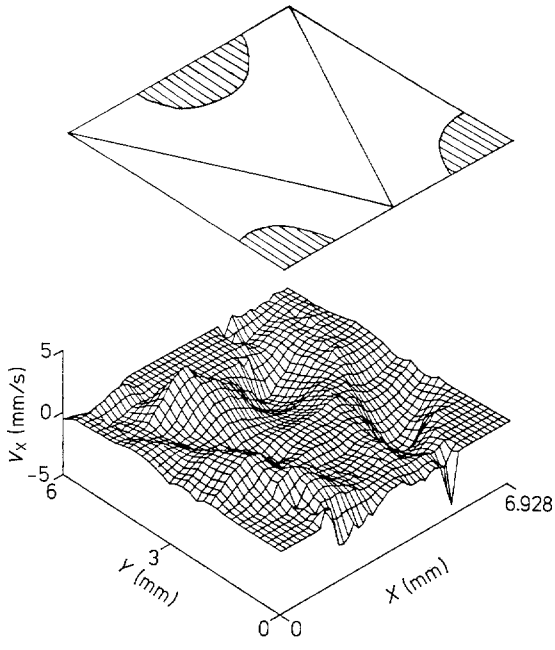

Fig. 9. Computed lateral directional velocity component at level 0.5 of model 1 ($Re = 0.494$)

cell. The coordinates of the 3-D graphics were chosen in such a way that the vertical Z-axis corresponds to the magnitude of the plotted component of the velocity vector. The two horizontal axes correspond to the original X and Y coordinates of the representative cell. The advantage of this procedure is that the flow field on a particular level can be presented as a whole, instead of presenting the data as velocity profiles at different locations. The plotting routines do not draw sections of the profile which are hidden from the view point. The view point can be altered to see any hidden section of the profile. However, for relative comparison between the velocity fields at different levels of the model porous medium, all plots were made from the same view point. Figure 8 is a sample 3-D graph of the vertical directional velocity component at level 0.5. Both positive and negative velocity components of the velocity field can be seen. As shown in Fig. 2, the cell geometry has only positive axes of the Cartesian volume and bulk flow was along the Y-axis in model 1 flow field, and it was along the X-axis in model 2 flow field. While plotting both vertical and lateral (refer to following paragraph) component velocities, velocity fields away from the origin of the model porous medium were considered positive, and velocity fields toward the origin were considered to be negative. The cross sectional layout of the cell geometry is depicted in all the figures for easy understanding of the velocity data.

The third unmeasured velocity component was then computed from the two measured components using a computer program (Yarlagadda 1986) developed for this purpose. In this program, first the continuous derivatives of the two known components were computed at each nodal point of the grid. Next, the derivative of the third component was derived from the continuity equation. Then, the third component was computed by integrating the estimated continuous derivatives of the third component. Zero velocity boundary conditions were applied at the walls of the glass rods. Figure 9 is a sample plot for the lateral directional velocity field plotted in 3-D graphical form. As shown in Fig. 9, the computer program estimated both positive and negative values. The accuracy of the third component generating program was established by using the program in a known three-dimensional velocity field (Yarlagadda 1986).

4 Results

Tables 1 and 2 show the experimental conditions of the flow fields studied. The friction factor ψ is computed from the following equation (Darcy 1856):

$$\psi = (\Delta P/L)\, d/(\varrho\, V^2/2)$$

where d is the diameter of the glass rods (3 mm), and V is the average velocity based on the volumetric flow rates per unit cross sectional area (based on empty chamber). Obviously at these flow conditions, the flow fields are in the laminar regime. Figures 10–12 show the velocity components obtained model 1 at a Reynolds number of 0.88. In each figure, the results of the measured flow fields are presented at all five levels of the geometry. Next to the velocity plots, are the sketches of the geometry of the representative cell at each

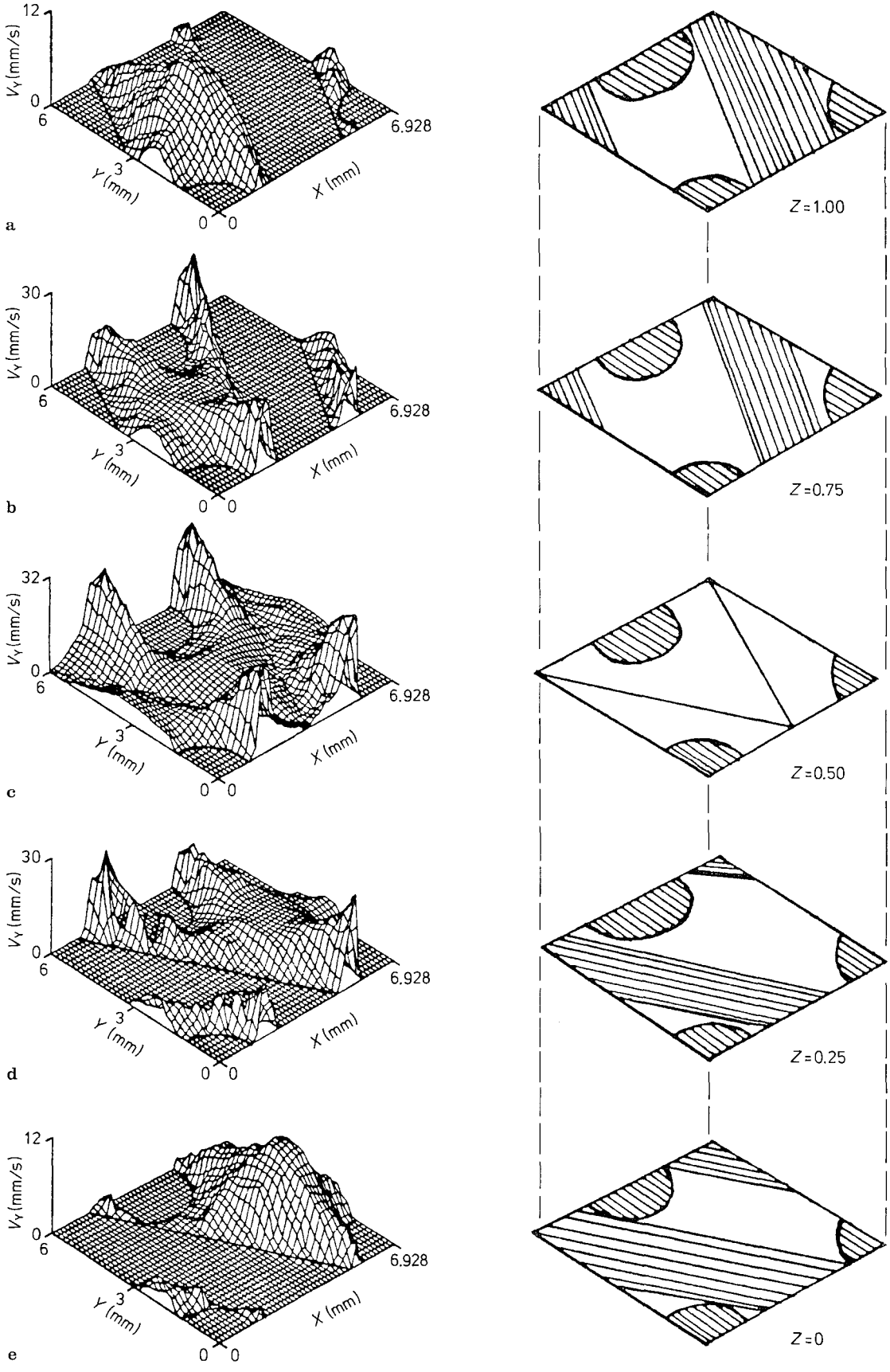

Fig. 10a–e. Bulk directional velocity component in model 1 ($Re = 0.88$)

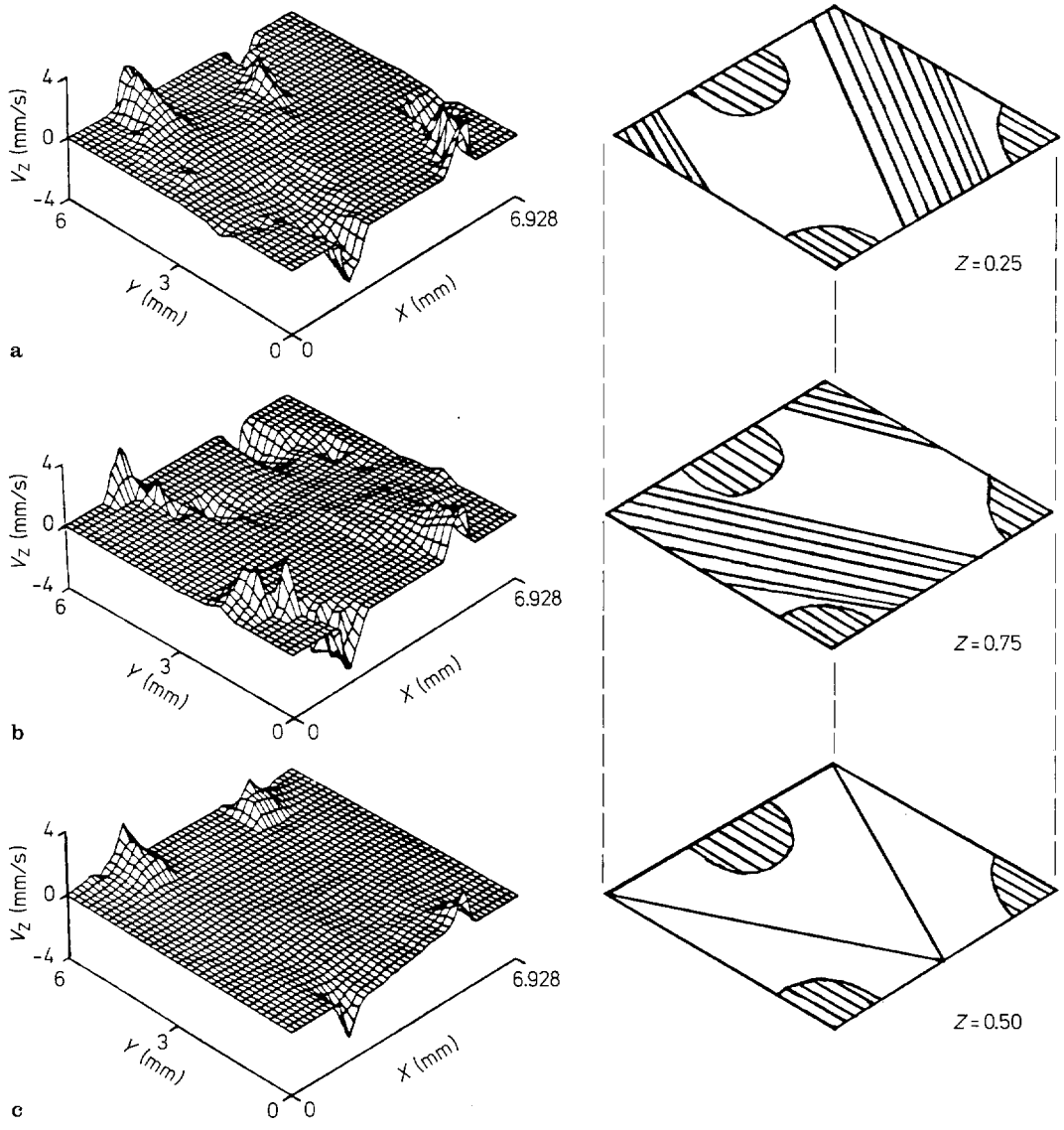

Fig. 11 a–c. Vertical directional velocity component in model 1 ($Re = 0.88$)

Table 1. Experimental conditions of 3-D flow fields in model 1 studies

S. no.	V (cm/s)	N_{Re}	ΔH (mm)	Log N_{Re}	Log ψ
1	0.540	0.327	5.00	−0.0555	3.0514
2	0.815	0.494	9.80	−0.2090	3.1055
3	1.019	0.618	13.50	−0.3063	3.1612
4	1.320	0.880	20.00	−0.4553	3.2257

Table 2. Experimental conditions of 3-D flow fields in model 2 studies

S. no.	V (cm/s)	N_{Re}	ΔH (mm)	Log N_{Re}	Log ψ
1	0.394	0.2626	2.90	−0.5807	3.200
2	1.093	0.7281	1.61	−0.1378	3.058
3	1.855	1.2366	3.87	0.0922	2.980
4	2.814	1.9140	8.55	0.2819	2.945

location. The figures (Fig. 11 and 14) showing the vertical directional velocity components have not plots made for levels 0 and 1.0. Zero vertical flow fields were recorded at these two levels which correspond to the top and bottom surfaces of the representative cell geometry (Fig. 2). Figures 13–15 show the velocity components obtained in model 2 at a Reynolds number of 0.914. The data corresponding to other three flow rates in both the models are not shown here due to space limitation. (For this data refer to Yarlagadda 1986).

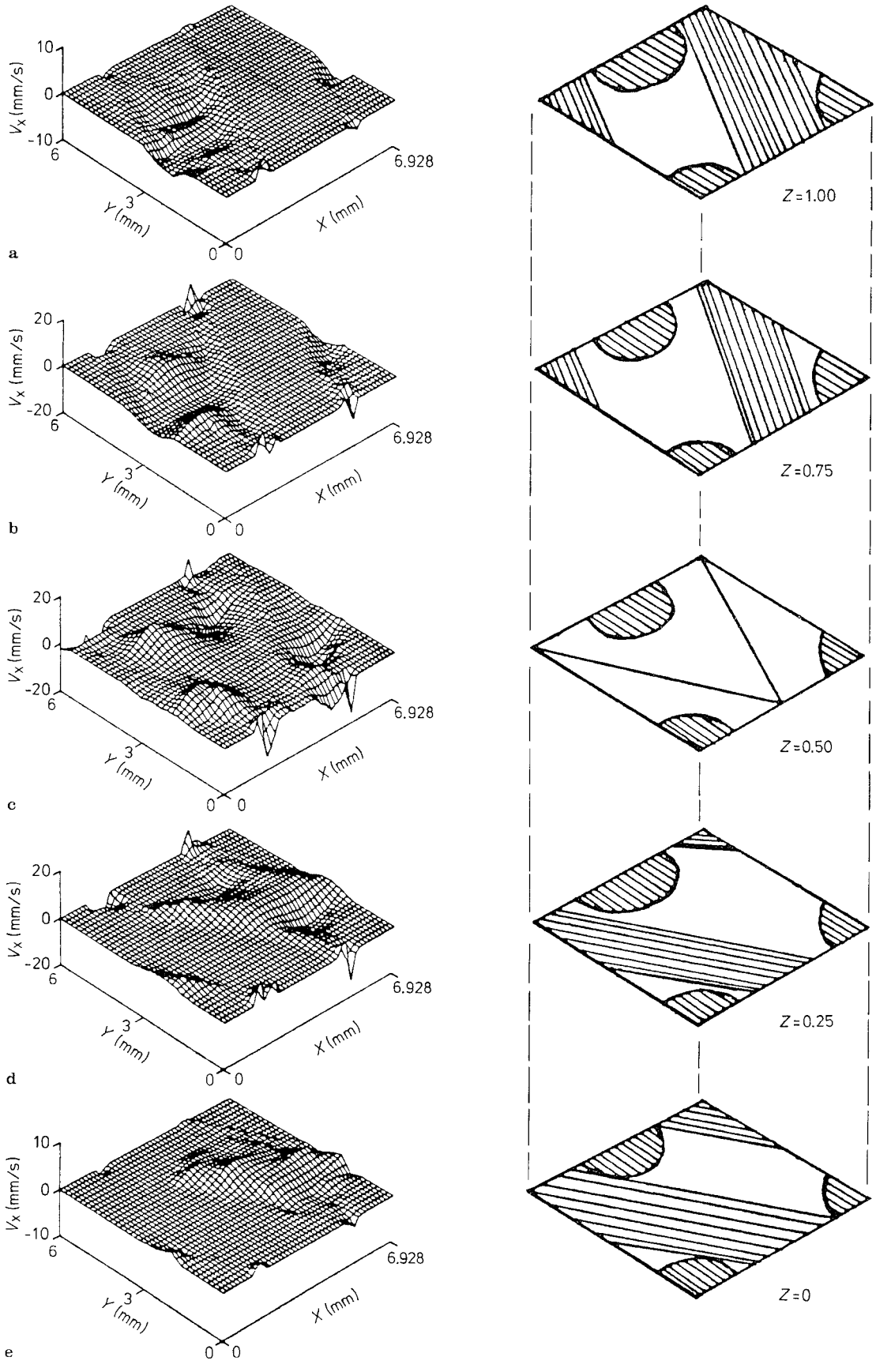

Fig. 12a–e. Computed lateral directional velocity component in model 1 ($Re = 0.88$)

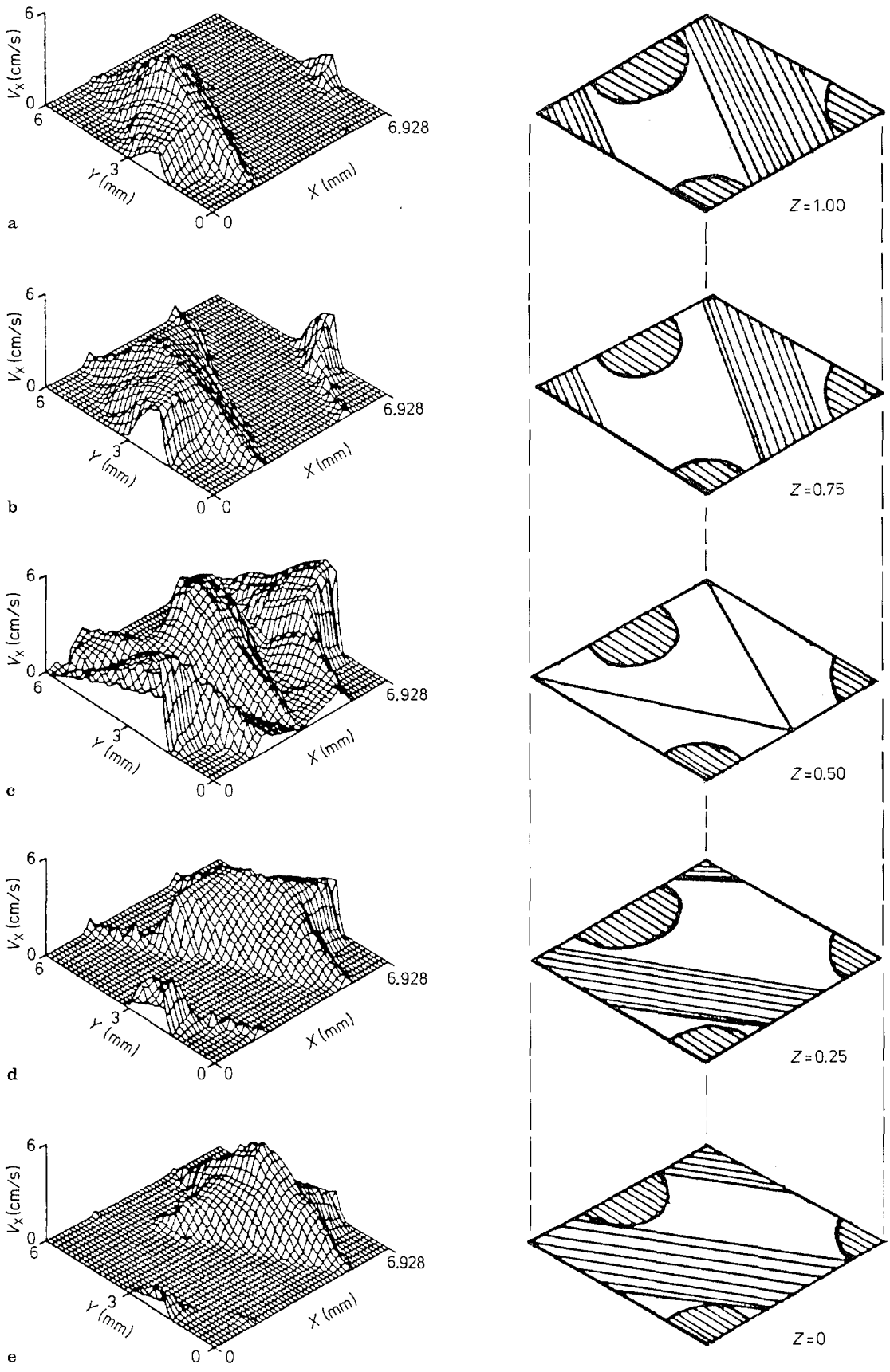

Fig. 13a–e. Bulk directional velocity component in model 2 ($Re = 1.914$)

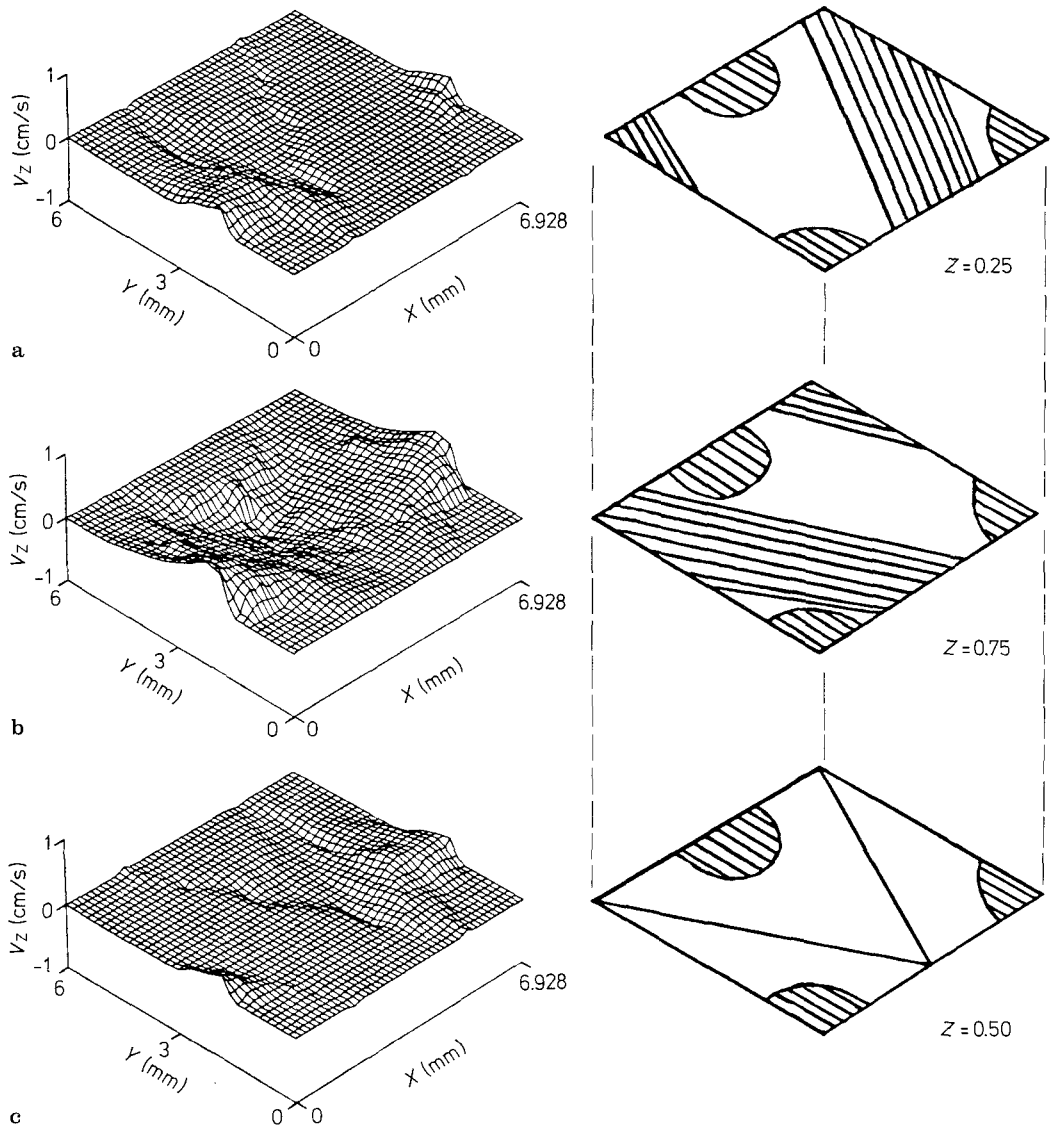

Fig. 14a–c. Vertical directional velocity component in model 2 ($Re = 1.914$)

5 Discussion

The success of the experiments described in this paper depended on a number of items. To start with, the quality of the glass rods used in the experiments was very important. Once the glass rods were cut to the size to fit into the model geometry the edges had to be annealed so that there would be no cut surface. If the ends of the glass rods were not properly annealed, there would be interference of the laser beams. The next important point was the isolation of the external vibration from being transmitted to the test sections. Since measuring the velocity components at the exact grid location was very important (grid location being separated by only 250 microns), any small vibrations transmitted to the test section might lead to erroneous results. The traversing mechanism of the test section had to be accurate. A small error (on the order of a few microns) in relocating the grid location would result in inaccurate results. Finally, the refractive index of the test fluid at the working temperature had to be exactly the same as that of the pyrex. Without achieving the absolute matching of the refractive index, it was not possible to obtain any valid measurements with the LDA system.

The measurements made in this experimental study indicate that the flow was very sensitive to the local geometry, and was changing the flow direction along the path of the flow. No negative velocity fields were recorded in the bulk flow direction. As seen in Fig. 10, in model 1 the bulk directional fluid movement was relatively high in the narrow gaps between the vertical and horizontal glass rods. Whereas in

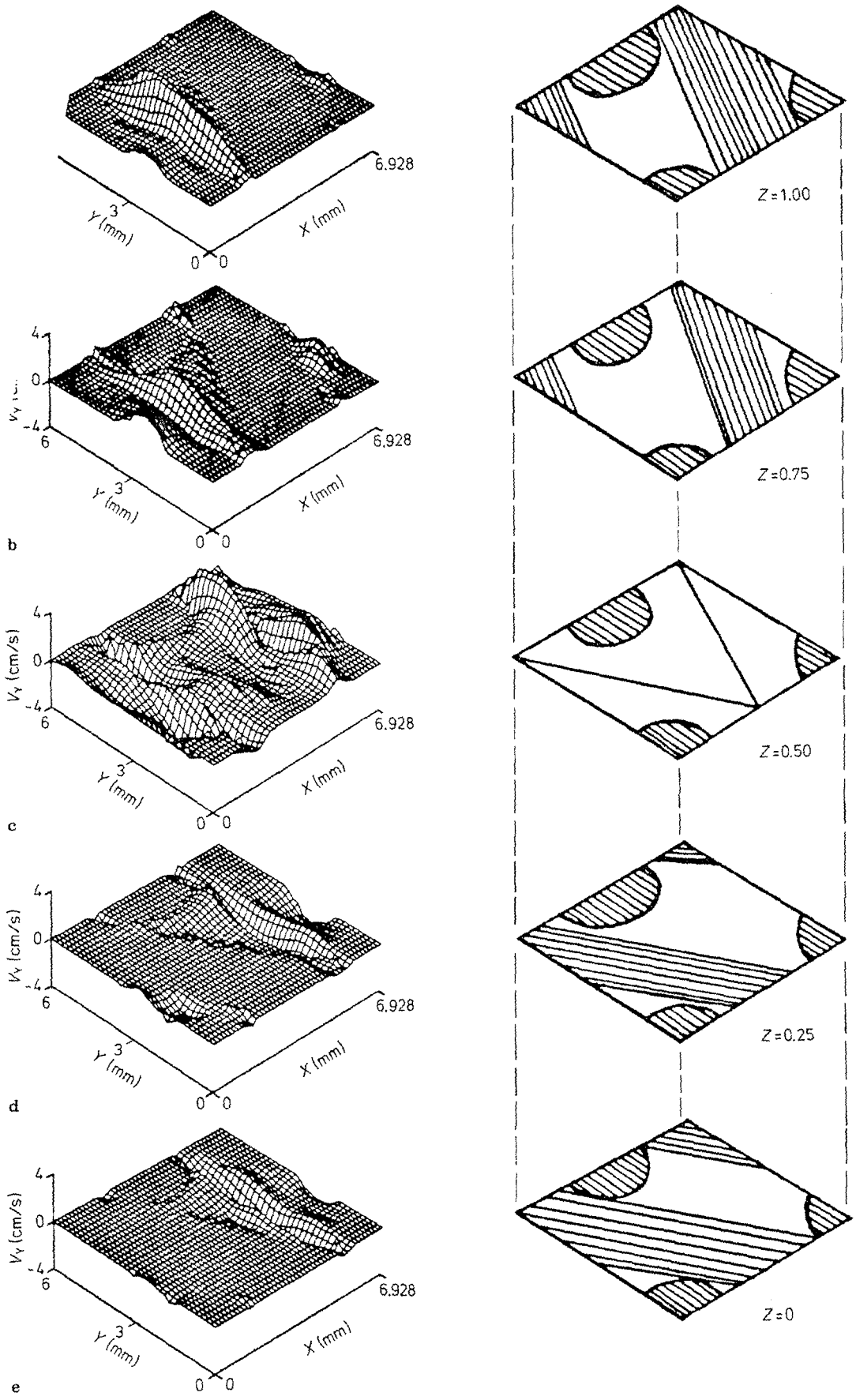

Fig. 15a–e. Computed lateral directional velocity component in model 2 ($Re = 1.914$)

model 2 (Fig. 13) no sharp peaks are seen at any location of the flow field. The data in model 2 also indicated that bulk flow direction fluid movement is very minimal in the gaps between the horizontal and vertical glass rods. By comparing the flow patterns at various levels, it can be observed that the velocities were zero near the walls of the horizontal glass rods. The flow fields at locations far away from the glass rods exhibit either flat or developing velocity fields. Accelerating and decelerating flow fields in the bulk flow direction indicate the presence of lateral or vertical directional velocity fields. In all these experiments the volumetric flow rates through the flow geometries were steady. Therefore, without lateral flow, such variations in velocities (velocity vector being constant at all locations of the test section) along the flow path that are seen at level 0.5 of Fig. 10 and 13 are not possible.

In the vertical direction, both positive and negative velocities can be seen at levels 0.25, 0.5, and 0.75 of the cell geometry. The same is not noticed at levels 0.0 and 1.0. This indicates that flow fields were moving upward and downward within the representative cell, but no such flow was present between layers of the representative cells. From this observation one can conclude that at these low Reynolds numbers, interlayer macro-mixing was absent (i.e. there is no fluid flow from the adjacent top and bottom cells to the representative cell under study). Also, there was some symmetry in the pattern of the flow fields. Figures 11 and 14 show the presence of an almost equivalent negative flow field existing at a mirror image location for every positive flow present in the flow field. In model 1 the vertical fluid movement was mainly in the narrow gaps between the vertical and horizontal glass rods (Fig. 11). Very small positive or negative vertical velocities were observed in the rest of the flow field. In the model 2 flow geometry (Fig. 14) vertical movement of the flow was mainly at locations that were away from the vertical glass rods. If the flow was approaching the upper half of the glass rod, the vertical directional velocity component was upwards (i.e. positive) and, if the flow was approaching the lower half of the glass rods, the vertical velocity component was downwards (i.e. negative). Similarly, the vertical velocity field in the back of the horizontal glass rods had either upward or downward velocity components, depending on whether the flow field was behind the lower half or upper half of the horizontal glass rods, respectively. In all cases, the vertical directional velocity component also increased with increasing bulk flow rates.

The computed lateral directional velocity fields (Fig. 12) clearly show velocity components in both negative and positive direction. The lateral velocity components were negative at the levels 1.0 and 0.75, and positive at levels 0.0 and 0.25. A combination of both positive and negative velocities as recorded at level 0.5. Similar phenomena were noticed in model 2 (Fig. 15). In both these models, the flow fields moved to the left of the bulk flow direction where the glass rods were oriented towards the left of the bulk flow direction. Similarly, the lateral direction velocity fields moved to the right in the layers where the horizontal glass rods were oriented toward the right of the bulk flow direction. These results indicate that the flow tended to follow the direction of the horizontal glass rods placed at an angle to the bulk flow direction. In model 1, the lateral velocity flow fields showed convergence behind the vertical glass rods. This phenomenon is clearly seen at level 0.5.

The general observations were that flow fields were steady at all locations with steady velocity components. The velocity vector had three components at all locations of the flow fields. The exception was at the top and bottom levels of the representative cell where the vertical directional velocity component was absent in both the models. Even though the flow fields took a tortuous path with both vertical and lateral directional movements, mixing of the fluid was absent. The absence of negative velocity fields in the bulk flow direction in both models infer that secondary vortices or eddy formation were absent over a range the flow rates studies ($N_{Re} < 1.914$).

The flow fields in models 1 and 2 are different mainly in two aspects. First, the bulk flow directional velocity fields in model 2 had no sharp peaks as were noticed in model 1. Secondly, in model 2 the velocity fields in the narrow gaps between the horizontal and vertical glass rods were either small or absent, whereas in model 1, the velocities were considerably higher at similar locations. This is mainly due to the difference in the orientation of the horizontal glass rods. In model 1 the horizontal rods were at an angle of 30° to the bulk flow direction, whereas, in the second model, they were at an angle of 60° to the bulk flow direction. Therefore, in model 2 the space in these gaps was not useful in transporting the fluids, although these spaces were important in model 1.

6 Conclusions

Matched refractive index technique along with the special apparatus used in this experimental study, made it possible to use LDA in a complicated test geometry. The model porous media made of 3 mm pyrex glass rods proved to be a good experimental test model for research studies. The absence of secondary vortices over the range of the flow rates studied shows that the viscous drag forces were dominant and the inertial effects were not noticeable. The two component velocities along the bulk flow direction and vertical direction were successfully measured using a 3 beam LDA system. The third unmeasured component was estimated from the two measured components and presented. The third component estimating program used the continuous velocity gradients of the two measured velocity components and the condition of continuity equation to estimate the continuous derivative of the third unmeasured component. The bulk direction flow fields had no negative velocity fields, but both vertical and lateral directional velocity fields had both positive and negative flow fields. There was no vertical

flow at top to bottom layers of the flow field, confirmed by zero vertical velocities at levels 0 and 1.0 of the representative cell. In the range on Reynolds numbers studied, fluid mixing was absent in both the models, although the fluid follows a tortuous path. The flow was sensitive to the local geometry of the test section. The narrow gaps between the vertical glass rods and the horizontal glass rods were not useful for transporting the fluid in model 2, but the same was very important in model 1.

Acknowledgements

The authors wish to thank Absorbent Technology, Johnson and Johnson, for providing a fellowship to carry out this work at the Georgia Institute of Technology, Atlanta, GA. Thanks to I. Moon for typing this manuscript.

References

Bear, J. 1972: Dynamics of fluids in porous media. New York: Elsevier

Carmen, P. C. 1956: Flow of gases through porous media. New York: Academic Press

Collins, R. E. 1961: Flow of fluids through porous materials. New York: Reinhold

Coulaud, O.; Morel, P.; Caltagirone, J. P. 1988: Numerical modelling of nonlinear effects in laminar flow through a porous medium. J. Fluid Mech. 190, 393–407

Darcy, H. 1856: Les fontaines publiques de la ville de Dijon. Paris: Dalmont

Ergun, S. 1952: Fluid flow through packed columns. Chem. Eng. Prog. 48, 93–98

Greenkorn, R. A. 1983: Flow phenomena in Porous Media. New York: Marcel Dekker

Happel, J.; Brenner, H. 1973: Low Reynolds number hydrodynamics. Leyden: Noordhoff

Hudson, H. E.; Roberts, R. E. 1952: An investigation into the transition of fluid flow in bundled glass rods. Proc 2nd Medw Conf. Fluid Mech. Eng. Ser. 31, 105–115

Keller, J. B. 1976: Effective behavior of hetrogenous media. In: Statistical mechanics and statistical methods in theory and application. (ed. Landman, U.). pp. 631–644. New York: Plenum Press

Lin, E. S. 1981: Fluid flow in complex cylindrical geometrices. Ph.D. Thesis. Univ. of Virginia

Rose, H. 1945: An investigation into the laws of flow of fluids through beds of granular materials. Appl. Mech. 153, 145–162

Rosenstein, N. D. 1980: Nonlinear laminar flow in a porous medium. Ph.D. Thesis. Case Western Reserve University

Scheidegger, A. E. 1974: The physics of flow through porous media. Toronto: Univ. of Toronto Press

Yarlagadda, A. P. 1986: Fluid flow in model capillary structures. Ph.D. Thesis. Atlanta/GA: Georgia Institute of Technology

Received May 5, 1989